

A backgate for enhanced tunability of holes in planar germanium

Luigi Ruggiero,^{*,†} Arianna Nigro,[†] Ilaria Zardo,^{†,‡} and Andrea Hofmann^{*,†,‡}

[†]*Physics Department, University of Basel, Klingelbergstrasse 82, CH-4055 Basel, Switzerland*

[‡]*Swiss Nanoscience Institute, Klingelbergstrasse 82, CH-4055 Basel, Switzerland*

E-mail: luigi.ruggiero@unibas.ch; andrea.hofmann@unibas.ch

Abstract

Planar semiconductor heterostructures offer versatile device designs and are promising candidates for scalable quantum computing. Notably, heterostructures based on strained germanium have been extensively studied in recent years, with emphasis on their strong and tunable spin-orbit interaction, low effective mass, and high hole mobility. However, planar systems are still limited by the fact that the shape of the confinement potential is directly related to the density. In this work, we present the successful implementation of a backgate for a planar germanium heterostructure. The backgate, in combination with a topgate, enables independent control over the density and the electric field, which determines important state properties such as the effective mass, the g -factor and the quantum lifetime. This unparalleled degree of control paves the way towards engineering qubit properties and facilitates the targeted tuning of bilayer quantum wells, which promise denser qubit packing.

Compressively strained Ge quantum wells (QWs) in SiGe heterostructures have become well known for their heavy-hole (HH) ground states which have interesting properties for applications in quantum computing¹⁻³ and research on hybrid superconductor/semiconductor

devices.^{4–6} In undoped Ge/SiGe heterostructures, hole mobilities of several million cm^2/Vs have been reached,^{7,8} larger than those achieved in Si. However, by controlling the charge density with a top barrier alone, the density and the location of the charges within the QW are always closely related. The states are pushed towards the top SiGe barrier and the confinement strength grows with density. The close vicinity of the confined states to the interface increases the importance of interface scattering and any finite wavefunction overlap with the SiGe barrier may lead to stronger decoherence mechanisms in qubit devices. Furthermore, the confinement potential and the electric field affect the amount of HH-light-hole (LH) splitting^{9,10} and influence important properties such as the effective mass,¹¹ the spin–orbit interaction¹² and the g -factor.^{10,13}

We introduce a backgate to planar Ge/SiGe heterostructures, aiming to independently tune the density and the location of the hole wavefunction within the QW. Backgates are routinely used in 2D material systems for a separate control of the density and displacement field^{14–17} and have been successfully applied to heterostructures for the purpose of increased device flexibility or measuring double QW devices.^{18–21} Integrating a backgate into a heterostructure is more intricate as the substrate is thick. It requires precise control over the thinning process so as to bring the backgate in close vicinity of the QW to achieve an appreciable field-effect.

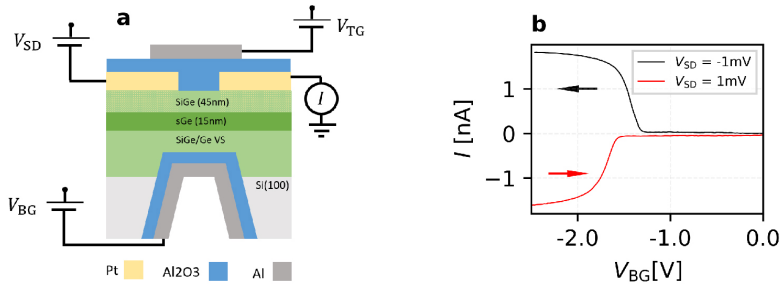


Figure 1: Single gate device characterization. (a) Sketch of the device and measurements setup. The flat region of the backgate is etched into the SiGe gradient buffer. (b) Accumulation curve of the current as a function of backgate voltage V_{BG} performed at 4 K on a device with a backgate and without a topgate. The two curves are measured with opposite polarity of the applied source-drain voltage V_{SD} and display sweeps in reverse direction.

Here, we make use of selective etching of the involved materials in order to place the backgate less than $1\text{ }\mu\text{m}$ below the QW, close enough to tune the two dimensional hole gas (2DHG) density with reasonable voltages. The heterostructure is schematically shown in Fig. 1(a). Its bottom layers consist of a thick Si substrate, a Ge virtual substrate, and a reverse-graded buffer to reach a constant composition of 80 % Ge in the barrier. The states of interest are the quasi-2D HH states in the Ge QW, which is confined from the top by another $\text{Si}_{0.2}\text{Ge}_{0.8}$ layer. The backgate is produced by wet etching the Si substrate with NaOH, an etchant that has a high selectivity to Si compared to Ge. The Al backgate is then fabricated on top of an insulating aluminium oxide layer. Ohmic contacts are fabricated from the top in order to measure the current induced in the 2DHG upon application of suitable gate voltages.

In a first step, we demonstrate the accumulation of a finite hole density within the Ge QW solely due to a backgate, i.e. in absence of any topgate. Fig. 1(b) shows the current I flowing due to a bias voltage V_{SD} as a function of voltage V_{BG} applied to the backgate when the sample is cooled to 4 K. As expected for an undoped heterostructure, no current is observed at zero backgate voltage. However, when sweeping V_{BG} negative, the current rises due to the accumulation of charges in the QW. When sweeping V_{BG} in reverse direction, the depletion occurs at slightly more negative voltages. This observation has also been made for topgated devices.²² In our case, the hysteresis is likely induced by charging of traps at imperfections in the bottom of the heterostructure or due to Ge segregation.²³ While the hysteresis is not always reversible at low temperatures, the original state is retrieved after a thermal cycle to room temperature. The two curves are obtained with opposite sign of V_{SD} and the equal magnitude of measured current demonstrates the absence of sizeable leakage between the ohmic contacts and the backgate. In fact, we do not observe leakage down to $V_{\text{BG}} = -7\text{ V}$.

Having demonstrated the charge accumulation with a backgate alone, we move on to build devices with back- and topgates, with the aim to individually tune the density and the

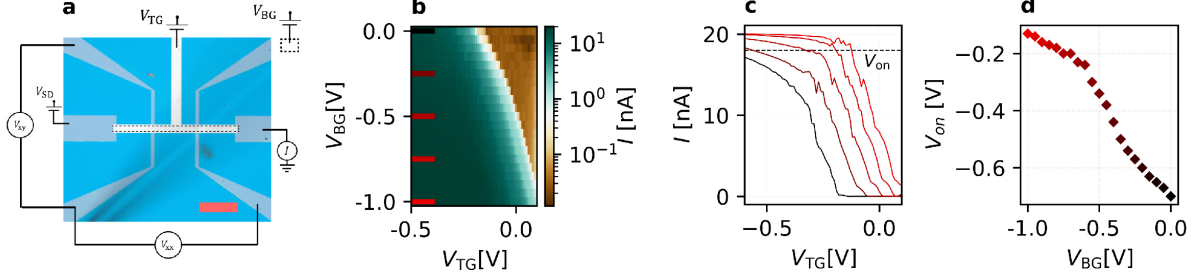


Figure 2: **Device details and accumulation curves with the top- and backgate.** (a) Confocal microscope picture of the hallbar device with a sketched measurement setup. The scale bar is 100 μm . The diagonal line is a bond-wire. (b) 2D map of accumulation curves as function of V_{TG} at different values of V_{BG} . (c) Traces at different V_{BG} marked in (b). V_{on} is defined as V_{TG} leading to 90 % of the saturation current. (d) V_{on} as a function of V_{BG} .

shape of the confinement potential. The optical micrograph in Fig. 2(a) depicts a top-view of the sample, showing the topgate in white color, ohmic contacts in grey and indicating the location of the backgate with dashed lines. The design of the sample is limited by our fabrication process allowing only rectangular backgates and a precision of 1 μm for the alignment between back and top. The backgate is slightly smaller than the topgate and the region of the 2DHG defined by the backgate is directly contacted with ohmic contacts. All of the following measurements are performed in a dilution refrigerator at base temperature of 10 mK unless noted otherwise.

We first characterize the relative size of the field effect of the two gates by measuring the current through the device as a function of top- and backgate voltages, see Fig. 2(b). The line-traces in Fig. 2(c) show how the accumulation curves obtained with the topgate change with the value of applied backgate voltage. To allow a quantitative comparison, we define V_{on} as the topgate voltage where the current equals 90 % of the saturation current. We compare in Fig. 2(d) V_{on} for different values of V_{BG} . The slope amounts to 0.5, suggesting that the backgate voltage has half the effect of the topgate voltage. This ratio is much bigger than our expectations based on the respective distances, d_{TG} and d_{BG} , of the gates to the QW with a ratio of $d_{BG}/d_{TG} > 10$.

In a different cooldown, we perform standard direct-current magnetotransport measure-

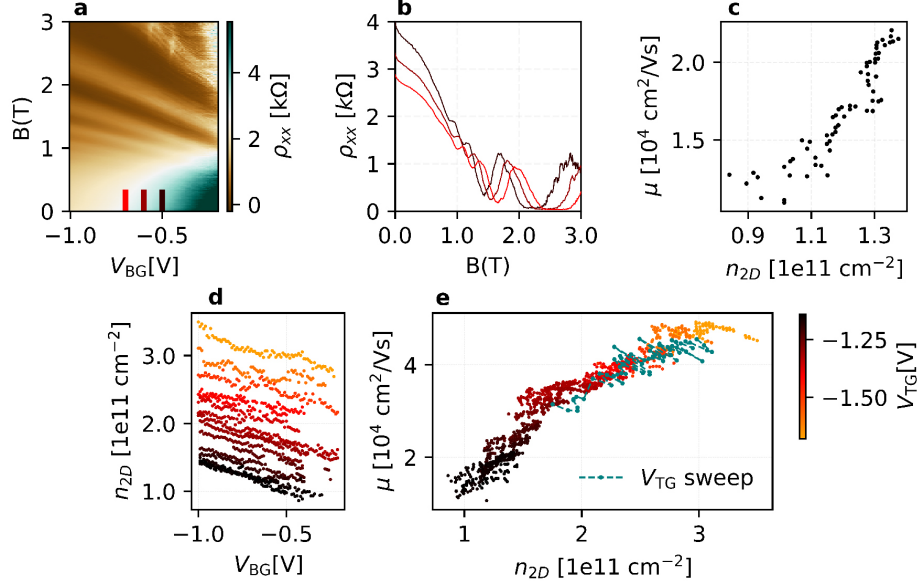


Figure 3: **Magnetotransport measurements with the V_{BG}** (a) ρ_{xx} as a function of V_{BG} and magnetic field B . (b) Traces along different V_{BG} as indicated in (a). (c) Mobility as a function of hole density. The density is extracted from Shubnikov–de Haas oscillations (SdH) oscillations in (a) and is then used for calculation of the mobility together with longitudinal resistance. (d) Densities as function of V_{BG} at different V_{TG} . (e) Mobility as a function of density extracted from measurements at varying V_{TG} . The data extracted with sweeping V_{BG} perfectly overlap with those obtained with V_{TG} at $V_{BG} = 0$ V.

ments to evaluate the efficiency of the backgate in tuning the 2DHG density. A Landau fan is shown in Figure 3(a), which has been recorded by only sweeping the backgate voltage and keeping V_{TG} at a constant value just before accumulation. The line traces in (b) demonstrate the quantization into Landau levels when the longitudinal resistivity plateaus at zero. The density is extracted from the period of the SdH at low fields and is then used to evaluate the mobility. As shown in Figure 3(c), the 2DHG density, n_{2D} , changes due to the voltage applied to the backgate. The mobility increases with density, which is typical in the low density regime, where particle scattering is still negligible compared to the effects of the potential homogeneity.

Aiming to further analyze the relative influence of the two gates onto the 2DHG, we perform magnetotransport measurements with increasingly negative values of V_{TG} . As shown in Figure 3(d), the density is linear in V_{BG} , demonstrating the field-effect induced by the

backgate. Overall, n_{2D} increases with more negative V_{TG} , as more charges are accumulated by the topgate. From these traces, the relative field effect of the backgate compared to the topgate is estimated as ~ 0.3 . Meanwhile, the effect of the two gates on the mobility is very similar, as illustrated in Figure 3(e). There, we analyze the same magnetotransport data as for panel (d) to extract the mobility obtained when sweeping the backgate at constant V_{TG} . For a comparison, the green datapoints display the mobility extracted from an independent measurement where the backgate is kept at ground and magnetotransport measurements have been performed using only the topgate (see supplementary data). The two sets of data are in perfect agreement, indicating that applying voltages to the backgate does not deteriorate the 2DHG.

Using both gates, however, changes the confinement potential which in turn may affect properties such as the effective mass m^* , the quantum lifetime τ_q and the g -factor of the states under investigation. In fact, the topgate alone produces a triangular confinement potential with the wavefunction pushed towards the top barrier. Using both gates allows for a more symmetric configuration as shown in the *nextnano* simulations of a simplified heterostructure in Figure 4(a).

We follow Ref.²⁴ to extract the effective mass m^* from the temperature-dependence of the SdH oscillations (see supplementary data) for a set configuration of top- and backgate voltages. Each data point in Figure 4(b) represents the average of the effective mass extracted at different values of magnetic fields and the standard deviation determines the error bar. The backgate is progressively changed while the topgate is adjusted to keep the density constant. Using the effective mass as input, we then extract^{7,24} the quantum lifetime τ_q and the g -factor as shown in Figure 4(b) and (c), respectively. We can discern a trend that m^* and τ_q increase while the g -factor decreases with the magnitude of the applied backgate voltage. A power-outage interrupted the measurements before all the high-field data for the g -factor could be measured.

In general, the properties of the ground state delicately depend on the confinement po-

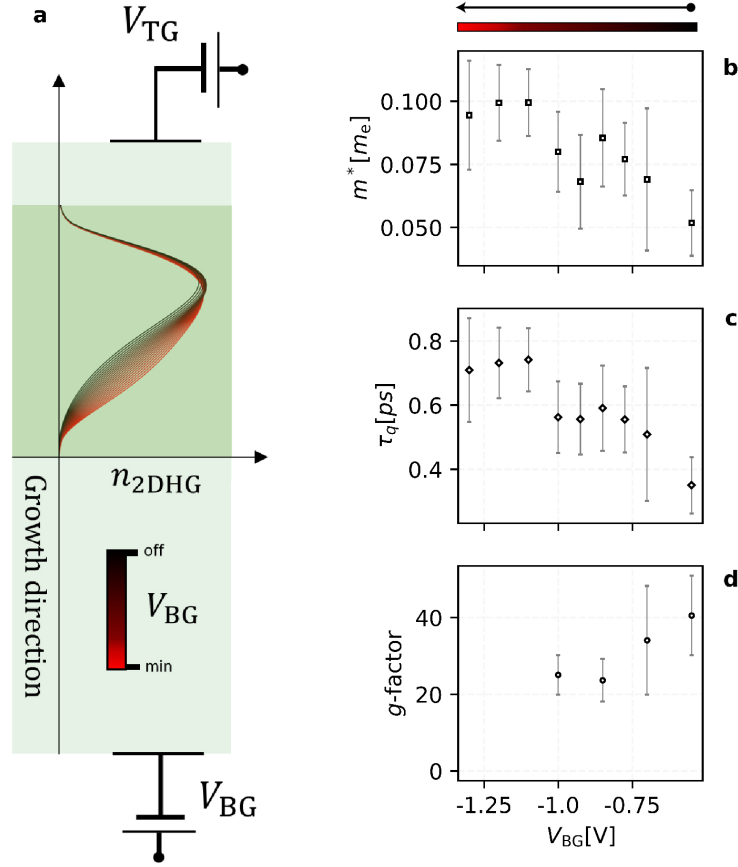


Figure 4: **Simulations and analysis of QW properties.** (a) Finite element simulations of a simplified strained Ge/SiGe heterostructure. Density curves for different backgate voltages (from 0 to the most negative values) at fixed topgate voltage. (b) Effective mass m^* , (c) quantum lifetime τ_q , (d) g -factor extraction for different values of V_{BG} at constant hole density.

tential and its symmetry.^{9,10,25} Recent simulations²⁶ have shown that the dependence of the g -factor on the applied electric field even depends on LH states not confined in the QW. Experimentally, it has been shown¹¹ that the effective mass decreases with density, i.e. with increasing confinement strength. This agrees well with our data, where m^* tends to grow when the confinement is weakened as the 2DHG is pulled away from the interface, see Figure 4(a).

In conclusion, we successfully integrated a backgate into a Ge/SiGe heterostructure, providing an alternative to the topgate for charge accumulation and density control of the 2DHG. By combining top- and backgates, we maintained a constant density and we observed a trend

towards a larger effective mass, smaller g -factor and increased quantum lifetime with a more negative backgate voltage. With the general nontrivial dependencies of state properties on the applied electric field, the backgate introduces an important knob for independently tuning the properties and the density. Such control will have important applications in qubit state engineering and, potentially, qubit manipulation. Furthermore the backgate facilitates precise control over bilayer QW devices and enables compressibility measurements. Bilayer QWs are receiving increased attention^{27,28} due to their potential for compact qubit packing, and measurements of the compressibility allow for conclusions about the density of states and the band structure.^{29,30}

Experimental

The backgate is fabricated by wet-etching the Si substrate with a 20 % NaOH in deionized water solution at 80 °C for 4 h. This leads to a complete removal of the 280 μm Si substrate and the Ge virtual substrate. During the etching process, the top surface is protected using a glass slide that is held in place with an O-Ring. The back is covered in plasma-enhanced chemical vapor deposition (CVD)-grown silicon nitride to which the mask is defined by standard photolithography techniques and dry etching in a reactive ion etching (RIE) using a mixture of CHF_3 and O_2 . As shown in the optical microscope and the confocal microscope images in Figure 5(a) and (b)-(c), respectively, the anisotropic etching causes the actual backgate region to be much smaller than the mask. After etching, the whole sample back is covered by aluminium oxide and a thick layer of aluminium which serves as the backgate electrode. The HAADF and EDX images show the angled etch profile and the flat bottom achieved with the NaOH etching. The etching anisotropy calls for a rectangular backgate shape and the thickness of remaining heterostructure limits the size of the backgate.

The same wet etching technique combined with RIE etching is applied to carve holes through the whole substrate, which serve as alignment marks. The achieved alignment

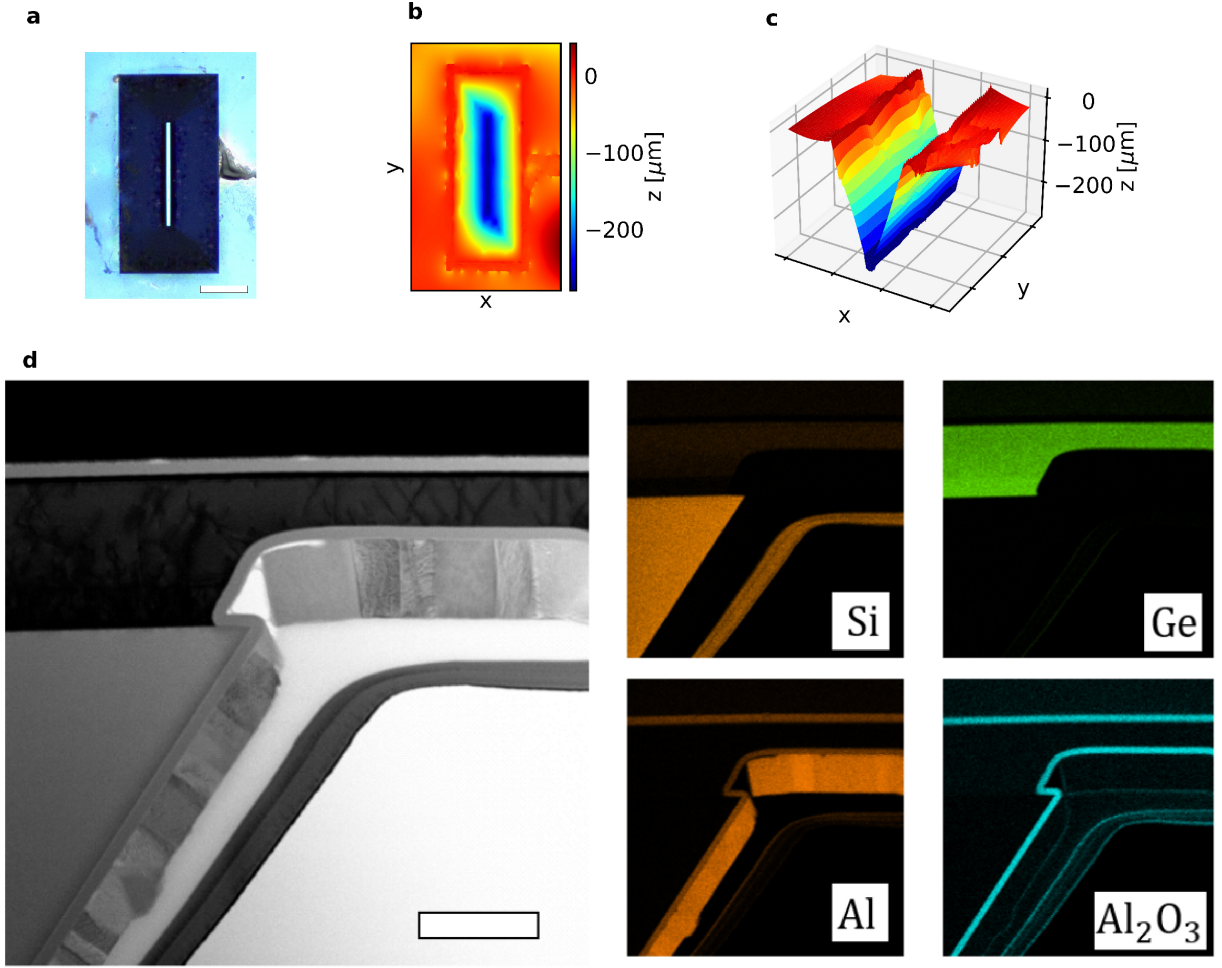


Figure 5: **Optical and scanning tunnelling microscopy (TEM) characterization.**(a) Confocal microscope image of the etched substrate defining the backgate region seen from the bottom. The scale bar is $200\text{ }\mu\text{m}$. (b) Height plot of (a), asymmetry along x -axis and spikes close to the edge of the etching are artifacts from the surface reflection. (c) Cut along (b) showing the typical anisotropic etching profile. (d) *left* High-angle annular dark-field (HAADF) image of a lamella cut performed perpendicular to the backgate region. The scale bar is $1\text{ }\mu\text{m}$. *right* Energy dispersive X-Ray (EDX) analysis of the backgate composition with the main materials involved.

precision is on the order of $1\text{ }\mu\text{m}$.

The heterostructure has been grown with CVD as described in Refs.^{31?} The platinum ohmic contacts and the aluminium topgate have been fabricated using standard photolithography and lift-off techniques as outlined in Refs.^{31?}

Acknowledgement

The authors thank Giulio de Vito for his contributions to the NaOH etching process, Christian Olsen and Christian Schönenberger for helpful discussions and Alexander Vogel and Marcus Wyss for assistance with the TEM and EDX images.

This work has been supported by the Swiss National Science Foundation through the NCCR SPIN (grant no. 51NF40-180604).

References

- (1) Scappucci, G.; Kloeffer, C.; Zwanenburg, F. A.; Loss, D.; Myronov, M.; Zhang, J.-J.; De Franceschi, S.; Katsaros, G.; Veldhorst, M. The Germanium Quantum Information Route. Nature Reviews Materials **2020**, 6, 926–943.
- (2) Jirovec, D. et al. A Singlet-Triplet Hole Spin Qubit in Planar Ge. Nature Materials **2021**, 20, 1106–1112.
- (3) Hendrickx, N. W.; Franke, D. P.; Sammak, A.; Scappucci, G.; Veldhorst, M. Fast Two-Qubit Logic with Holes in Germanium. Nature **2020**, 577, 487–491.
- (4) Hendrickx, N. W.; Franke, D. P.; Sammak, A.; Kouwenhoven, M.; Sabbagh, D.; Yeoh, L.; Li, R.; Tagliaferri, M. L. V.; Virgilio, M.; Capellini, G.; Scappucci, G.; Veldhorst, M. Gate-Controlled Quantum Dots and Superconductivity in Planar Germanium. Nature Communications **2018**, 9, 2835.
- (5) Aggarwal, K.; Hofmann, A.; Jirovec, D.; Prieto, I.; Sammak, A.; Botifoll, M.; Martí-Sánchez, S.; Veldhorst, M.; Arbiol, J.; Scappucci, G.; Danon, J.; Katsaros, G. Enhancement of Proximity-Induced Superconductivity in a Planar Ge Hole Gas. Physical Review Research **2021**, 3, L022005.
- (6) Vigneau, F.; Mizokuchi, R.; Zanuz, D. C.; Huang, X.; Tan, S.; Maurand, R.; Frolov, S.;

- Sammak, A.; Scappucci, G.; Lefloch, F.; De Franceschi, S. Germanium Quantum-Well Josephson Field-Effect Transistors and Interferometers. Nano Letters **2019**, 19, 1023–1027.
- (7) Lodari, M.; Kong, O.; Rendell, M.; Tosato, A.; Sammak, A.; Veldhorst, M.; Hamilton, A. R.; Scappucci, G. Lightly Strained Germanium Quantum Wells with Hole Mobility Exceeding One Million. Applied Physics Letters **2022**, 120, 122104.
- (8) Myronov, M.; Kycia, J.; Waldron, P.; Jiang, W.; Barrios, P.; Bogan, A.; Coleridge, P.; Studenikin, S. Holes Outperform Electrons in Group IV Semiconductor Materials. Small Science **2023**, 3, 2200094.
- (9) Winkler, R. Spin–Orbit Coupling Effects in Two-Dimensional Electron and Hole Systems; Springer Tracts in Modern Physics; Springer Berlin Heidelberg: Berlin, Heidelberg, 2003; Vol. 191.
- (10) Terrazos, L. A.; Marcellina, E.; Wang, Z.; Coppersmith, S. N.; Friesen, M.; Hamilton, A. R.; Hu, X.; Koiller, B.; Saraiva, A. L.; Culcer, D.; Capaz, R. B. Theory of Hole-Spin Qubits in Strained Germanium Quantum Dots. Physical Review B **2021**, 103, 125201.
- (11) Lodari, M.; Tosato, A.; Sabbagh, D.; Schubert, M. A.; Capellini, G.; Sammak, A.; Veldhorst, M.; Scappucci, G. Light Effective Hole Mass in Undoped Ge/SiGe Quantum Wells. Physical Review B **2019**, 100, 041304.
- (12) Stano, P.; Loss, D. Heavy-Hole–Light-Hole Mixing at the Zone Center. 2024.
- (13) Ivchenko, E. L.; Kiselev, A. A.; Willander, M. Electronic g Factor in Biased Quantum Wells. Solid State Communications **1997**, 102, 375–378.
- (14) Novoselov, K. S.; Geim, A. K.; Morozov, S. V.; Jiang, D.; Zhang, Y.; Dubonos, S. V.;

- Grigorieva, I. V.; Firsov, A. A. Electric Field Effect in Atomically Thin Carbon Films. Science **2004**, 306, 666–669.
- (15) Oostinga, J. B.; Heersche, H. B.; Liu, X.; Morpurgo, A. F.; Vandersypen, L. M. K. Gate-Induced Insulating State in Bilayer Graphene Devices. Nature Materials **2008**, 7, 151–157.
- (16) Mak, K. F.; Lui, C. H.; Shan, J.; Heinz, T. F. Observation of an Electric-Field-Induced Band Gap in Bilayer Graphene by Infrared Spectroscopy. Physical Review Letters **2009**, 102, 256405.
- (17) Zhang, Y.; Tang, T.-T.; Girit, C.; Hao, Z.; Martin, M. C.; Zettl, A.; Crommie, M. F.; Shen, Y. R.; Wang, F. Direct Observation of a Widely Tunable Bandgap in Bilayer Graphene. Nature **2009**, 459, 820–823.
- (18) Eisenstein, J. P.; Pfeiffer, L. N.; West, K. W. Independently Contacted Two-Dimensional Electron Systems in Double Quantum Wells. Applied Physics Letters **1990**, 57, 2324–2326.
- (19) Weckwerth, M. V.; Simmons, J. A.; Harff, N. E.; Sherwin, M. E.; Blount, M. A.; Baca, W. E.; Chui, H. C. Epoxy Bond and Stop-Etch (EBASE) Technique Enabling Backside Processing of (Al)GaAs Heterostructures. Superlattices and Microstructures **1996**, 20, 561–567.
- (20) Rubel, H.; Fischer, A.; Dietsche, W.; Von Klitzing, K.; Eberl, K. Fabrication of Independently Contacted and Tuneable 2D-electron-hole Systems in GaAs/AlGaAs Double Quantum Wells. Materials Science and Engineering: B **1998**, 51, 207–211.
- (21) Berl, M.; Tiemann, L.; Dietsche, W.; Karl, H.; Wegscheider, W. Structured Back Gates for High-Mobility Two-Dimensional Electron Systems Using Oxygen Ion Implantation. Applied Physics Letters **2016**, 108, 132102.

- (22) Massai, L.; Hetényi, B.; Mergenthaler, M.; Schupp, F. J.; Sommer, L.; Paredes, S.; Bedell, S. W.; Harvey-Collard, P.; Salis, G.; Fuhrer, A.; Hendrickx, N. W. Impact of Interface Traps on Charge Noise, Mobility and Percolation Density in Ge/SiGe Heterostructures. **2023**,
- (23) Wan, H.-W.; Cheng, Y.-T.; Cheng, C.-K.; Hong, Y.-J.; Chu, T.-Y.; Chang, M.-T.; Hsu, C.-H.; Kwo, J.; Hong, M. High-Ge-Content Si_{1-x}Ge_x Gate Stacks with Low-Temperature Deposited Ultrathin Epitaxial Si: Growth, Structures, Low Interfacial Traps, and Reliability. ACS Applied Electronic Materials **2022**, 4, 2641–2647.
- (24) Lei, Z.; Lehner, C. A.; Rubi, K.; Cheah, E.; Karalic, M.; Mittag, C.; Alt, L.; Scharnetzky, J.; Märki, P.; Zeitler, U.; Wegscheider, W.; Ihn, T.; Ensslin, K. Electronic g -Factor and Magnetotransport in InSb Quantum Wells. Physical Review Research **2020**, 2, 033213.
- (25) Bir, G. L.; Bir, G. L.; Pikus, G. E.; Pikus, G. E.; Bir, G. L. Symmetry and Strain-Induced Effects in Semiconductors; A Halsted Press Book; Wiley [u.a.]: New York, 1974.
- (26) Wang, C.-A.; Scappucci, G.; Veldhorst, M.; Russ, M. Modelling of Planar Germanium Hole Qubits in Electric and Magnetic Fields. 2022.
- (27) Tosato, A.; Ferrari, B.; Sammak, A.; Hamilton, A. R.; Veldhorst, M.; Virgilio, M.; Scappucci, G. A High-Mobility Hole Bilayer in a Germanium Double Quantum Well. Advanced Quantum Technologies **2022**, 5, 2100167.
- (28) Tidjani, H.; Tosato, A.; Ivlev, A.; Déprez, C.; Oosterhout, S.; Stehouwer, L.; Sammak, A.; Scappucci, G.; Veldhorst, M. Vertical Gate-Defined Double Quantum Dot in a Strained Germanium Double Quantum Well. Physical Review Applied **2023**, 20, 054035.

- (29) Eisenstein, J. P.; Pfeiffer, L. N.; West, K. W. Negative Compressibility of Interacting Two-Dimensional Electron and Quasiparticle Gases. Physical Review Letters **1992**, 68, 674–677.
- (30) Henriksen, E. A.; Eisenstein, J. P. Measurement of the Electronic Compressibility of Bilayer Graphene. Physical Review B **2010**, 82, 041412.
- (31) Nigro, A.; Jutzi, E.; Forrer, N.; Hofmann, A.; Gadea, G.; Zardo, I. High Quality Ge Layers for Ge/SiGe Quantum Well Heterostructures Using Chemical Vapor Deposition. Physical Review Materials **2024**, 8, 066201.

Supporting Information Available

Supplementary S1: Hall density

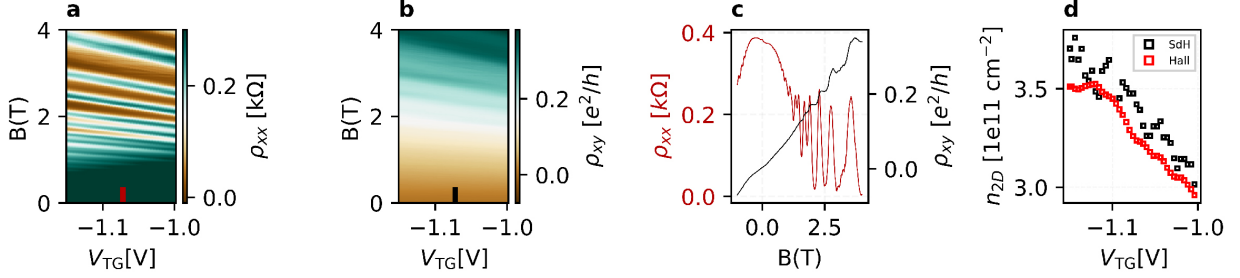


Figure 6: **Comparison of extracted Hall and SdH density.** (a-b) hall measurements showing ρ_{xx} and ρ_{xy} as function of V_{TG} . (c) Line trace cut along the respective 2D maps for ρ_{xx} and ρ_{xy} . (d) Extracted density of holes from both SdH oscillations and hall resistivity.

Figure 6 shows a comparison of the hole density extracted from Hall resistivity and SdH oscillations. Figure 6(a) and (b) respectively show ρ_{xx} and ρ_{xy} maps as a function of V_{TG} and B , with voltage dependent plateaus and SdH oscillations. The line traces in Figure 6(c) highlight a small mixing of longitudinal and transversal component: a slight asymmetry around zero field for ρ_{xx} and non-linearity in ρ_{xy} . Nevertheless, the extracted densities agree very well, as shown in Figure 6(d). The mixing could well be an artifact from the gate design which is not optimal for measuring the Hall effect. Since, with our gate design, the longitudinal resistivity is more reliable, we extract the density from SdH oscillations throughout the whole work.

Supplementary S2: V_{TG} sweep

We show in Figure 7(a) the magnetotransport measurements obtained using only the topgate with the backgate voltage fixed at 0 V. The density is obtained from the SdH oscillations and plotted as a function of V_{TG} in Figure 7(b). The mobility, shown in Figure 7(c) is evaluated using $\rho_{xx}(B = 0)$ and the density. As discussed in the main text, the mobility versus density

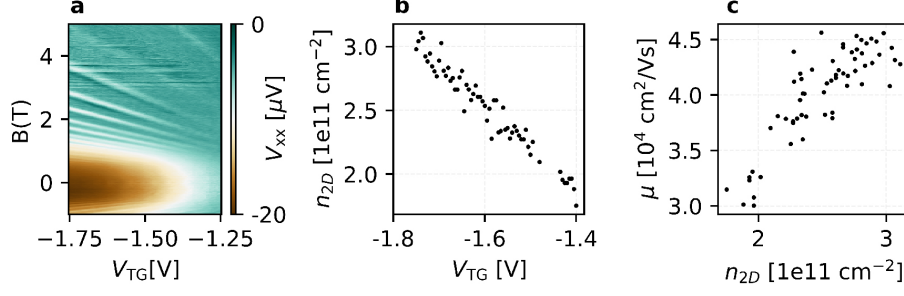


Figure 7: **Magnetotransport measurements sweeping V_{TG} .** (a) 2D map of V_{xx} as function of V_{TG} . (b-c) Extracted density and related mobility

behaviour is independent of the gate used to measure the data.

Supplementary S3: Fitting routines for m^* and τ_q

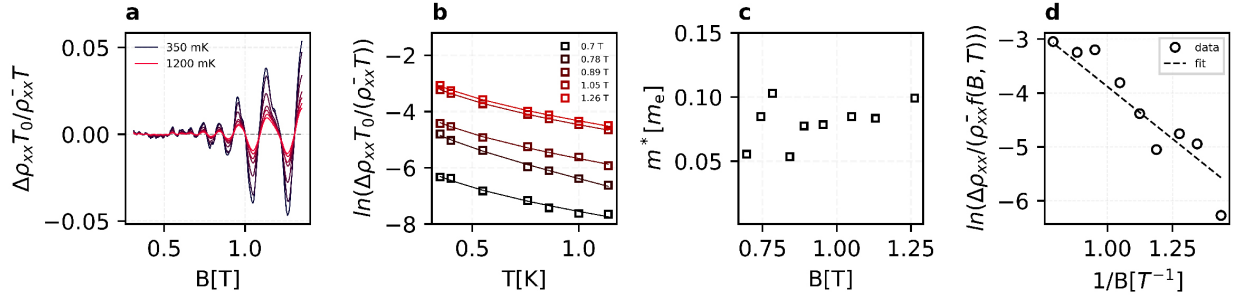


Figure 8: **QW properties fitting procedure.** (a) SdH with removed magnetoresistance background for varying temperatures. (b) Fit of the envelope function for different filling factors (only selected magnetic field values shown). (c) Extracted effective mass m^* for different filling factors. (d) Fit of the envelope function at lowest temperature in order to extract τ_q .

Figure 8 displays the additional data used for fitting m^* and τ_q as described in Ref.²⁴